

Phase diagram and critical properties of a two-dimensional associating lattice gas

I. Ibagon ^{1,*}, A. P. Furlan ^{1,†}, T. J. Oliveira ^{2,‡} and R. Dickman ^{3,§}

¹*Departamento de Física, ICEx, Universidade Federal de Minas Gerais, C.P. 702, 30123-970, Belo Horizonte, Minas Gerais-Brazil*

²*Departamento de Física, Universidade Federal de Viçosa, 36570-900, Viçosa, Minas Gerais, Brazil*

³*Departamento de Física and National Institute of Science and Technology for Complex Systems, ICEx, Universidade Federal de Minas Gerais, C.P. 702, 30123-970 Belo Horizonte, Minas Gerais-Brazil*



(Received 4 October 2021; accepted 1 December 2021; published 15 December 2021)

We revisit the associating lattice gas (ALG) introduced by Henriques *et al.* [*Phys. Rev. E* **71**, 031504 (2005)] in its symmetric version. In this model, defined on the triangular lattice, interaction between molecules occupying nearest-neighbor sites depends on their relative orientation, mimicking the formation of hydrogen bonds in network-forming fluids. Although all previous studies of this model agree that it has a disordered fluid (DF), a low-density liquid (LDL), and a high-density liquid (HDL) phase, quite different forms have been reported for its phase diagram. Here, we present a thorough investigation of its phase behavior using both transfer matrix calculations and Monte Carlo (MC) simulations, along with finite-size scaling extrapolations. Results in striking agreement are found using these methods. The critical point associated with the DF-HDL transition at full occupancy, identified by Furlan *et al.* [*Phys. Rev. E* **100**, 022109 (2019)] is shown to be one terminus of a *critical line* separating these phases. In opposition to previous simulation studies, we find that the transition between the DF and LDL phases is always discontinuous, similar to the LDL-HDL transition. The associated coexistence lines meet at the point where the DF-HDL critical line ends, making it a critical-end-point. Overall, the form of the phase diagram observed in our simulations is very similar to that found in the exact solution of the model on a Husimi lattice. Our results confirm that, despite the existence of some waterlike anomalies in this model, it is unable to reproduce key features of the phase behavior of liquid water.

DOI: [10.1103/PhysRevE.104.064120](https://doi.org/10.1103/PhysRevE.104.064120)

I. INTRODUCTION

The importance water has to life on Earth is perhaps comparable to the degree of unusual behavior this liquid displays. In fact, when compared with other substances, liquid water presents a number of anomalies (such as in density, diffusivity, and so on), which are believed to originate in the particular manner in which H₂O molecules interact, through hydrogen bonds forming a local, approximately tetrahedral network [1]. The three main scenarios proposed to understand water, viz. the stability-limit [2], the singularity-free [3], and liquid-liquid critical point (LLCP) [4] hypotheses, are all consistent with the presence of such a network. The later scenarios are based on the fact that just as ice becomes glassy and can exist in low- and high-density amorphous phases [5], the continuation of these phases (increasing the temperature T above that of spontaneous crystallization) may give rise to a low-density liquid (LDL) and a high-density liquid (HDL) phase [1,6]. Although there is some indirect experimental evidence for the existence of the LLCP [7–9], including some coming from water in nanopores [10–13], a definitive proof is still lacking [14], mainly because the LLCP would exist in the metastable,

deeply supercooled region, which is very difficult to access experimentally in bulk water.

In this context, much of this debate has been based on computational studies, with several realistic models for water confirming the LLC hypothesis (see Ref. [15] for a recent review). A number of simplified associating lattice gas (ALG) models, designed to possess two liquid phases, have also been introduced in two [16–22] and three dimensions [3,23–33]. These ALG models usually feature an attractive, orientation-dependent interaction between molecules occupying nearest neighbor (NN) sites—mimicking the hydrogen bonding in network forming fluids—competing with a repulsive excluded-volume interaction. Phase diagrams displaying a LLC have been reported for some of these models [21,22,27–30,32,33], though latter works on some these models have demonstrated a phase behavior without a LLC [21,22,33].

An example of this is the symmetric version of the Besseling and Lyklema model [26], firstly analyzed by Girardi *et al.* [33]. This model is defined on the body-centered cubic lattice, where each molecule can form up to four hydrogen bonds with NNs, similar to H₂O. While these bonds lower their energy, nonbonding molecules at NN sites experience a repulsive “van der Waals” interaction. Beyond the GAS-liquid coexistence line ending at a critical point, a LDL-HDL coexistence line ending at a second critical point was also reported in Ref. [33], yielding a phase diagram qualitatively similar to the one in Fig. 1(a). (As an aside, we remark that the phase commonly called GAS in the literature related to these models will be

*ibagon@fisica.ufmg.br

†apfurlan@fisica.ufmg.br

‡tiago@ufv.br

§dickman@fisica.ufmg.br

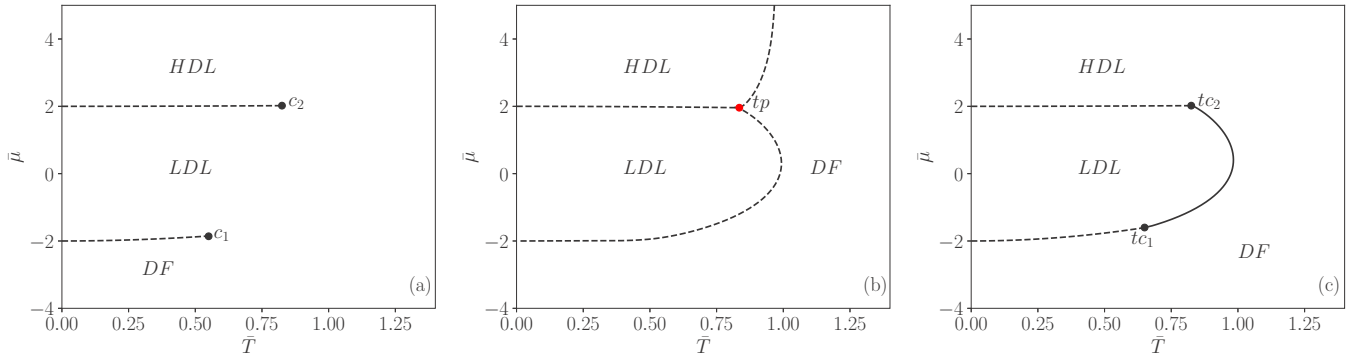


FIG. 1. Qualitative phase diagrams for the symmetric H&B model in the (reduced) $\bar{\mu}$ - \bar{T} plane adapted from Refs. [22,34,35] in panels (a), (b), and (c), respectively. Solid and dashed lines represent continuous and discontinuous phase transitions, respectively. The coexistence points at $T = 0$ are exact, while the loci of the critical points c_1 and c_2 , of the triple point tp , and of the tricritical points tc_1 and tc_2 are those found numerically in the references cited above.

regarded as a *disordered fluid* (DF) here, since it may extend to large chemical potentials and so, high densities.) Subsequent studies of this ALG [36–38], notwithstanding, revealed a much more complex phase behavior, with the LLCP [c_2 in Fig. 1(a)] being actually a tricritical point, while c_1 is disputed as being a critical-end-point [36,37] or a bicritical point [38]. These works also uncovered a critical line separating the HDL and DF phases [36–38].

A similar sequence of events marks the history of the ALG model introduced by Henriques and Barbosa (H&B) [21] which is a nonsymmetric two-dimensional (2D) version of the 3D model analyzed by Girardi *et al.* [33]. The H&B model is defined on the triangular lattice, in which each molecule has four bonding arms (two donors and two acceptors of protons), beyond two inert arms separated by 180° . In their original Monte Carlo analysis, H&B [21] reported a phase diagram analogous to that in Fig. 1(a), with two coexistence lines and two critical points. Further work on this model indicated, however, a different and richer phase diagram, with two additional continuous transition lines: DF-LDL and DF-HDL [39]. In this phase diagram, the DF-LDL coexistence line ends at a tricritical point where it meets the DF-LDL continuous line; and the LDL-HDL coexistence line ends at a bicritical point where it meets the continuous DF-LDL and DF-HDL lines [39].

Several modifications of the H&B model have been proposed [22,35,40]. Of particular interest here is the symmetric version introduced by Balladares *et al.* [22], in which no distinction is made between donor and acceptor arms. The literature on this symmetric ALG is also marked by controversy. For example, the original MC simulations of Ref. [22] again suggested the phase behavior of Fig. 1(a), consistent with the LLCP hypothesis. The semi-analytical mean-field solution of this simplified version of the H&B model on a Husimi lattice built with hexagonal plaquettes [34] revealed a qualitatively different phase diagram, with three coexistence lines (DF-HDL, DF-LDL and LDL-HDL) meeting at a triple point (tp), as shown in Fig. 1(b). Later MC simulations [35] supported the phase behavior of Fig. 1(c), with two coexistence lines (DF-LDL and LDL-HDL) ending at two tricritical points (tc_1 and tc_2), which are linked by a critical DF-LDL

line. No transition between the HDL phase and the disordered fluid was reported in Ref. [35].

More recently, this symmetric H&B model was investigated in the limit of full occupancy (corresponding to a chemical potential $\mu \rightarrow \infty$) using MC simulations and semi-analytical solutions on Husimi lattices [41]. The simulations yielded a continuous transition between the HDL and the DF phase at a (reduced) temperature $\bar{T}_c = 0.9525(5)$, with critical exponents and Binder cumulant in good agreement with those of the three-state Potts model in 2D [42]. However, the Husimi lattice solutions furnish a discontinuous transition, as a continuation of the DF-HDL coexistence line found for finite μ [34] to the limit of $\mu \rightarrow \infty$. All these results raise important questions on the phase behavior of this model: (i) Does it indeed exhibit a LLCP as in Fig. 1(a)? (ii) What is the true nature of the DF-LDL transition? Is it discontinuous as in Fig. 1(b) or does it have a tricritical point and a continuous part like in Fig. 1(c)? (iii) Assuming that a transition line does indeed exist separating the DF and HDL phases: Is it always discontinuous but ends at a critical point in the limit $\mu \rightarrow \infty$? Or does it start discontinuous and change to continuous at some finite μ ? Or, even, is the entire line continuous?

In this work we address these points through an extensive numerical study of this ALG model using both transfer-matrix analysis and MC simulations in the grand-canonical ensemble. Consistent results are obtained from both methods, demonstrating that the correct topology of the phase diagram is that of Fig. 1(b). However, in contrast with the mean-field result [34] shown in this figure, we find that the transition between the DF and HDL phases is always continuous and the critical DF-HDL line ends at a critical-end-point, where it meets the DF-LDL and LDL-HDL coexistence lines. The critical properties of the continuous transition line—an interesting problem scarcely tackled in the literature of lattice models for water (see Ref. [41] for a discussion)—are also investigated and an intriguing behavior is found, with some quantities presenting a close agreement with the three-state Potts class, while others have a large deviation from it.

The paper is organized as follows. In Sec. II, we present the investigated model. The transfer-matrix method and the associated results are discussed in Sec. III. A similar thing is

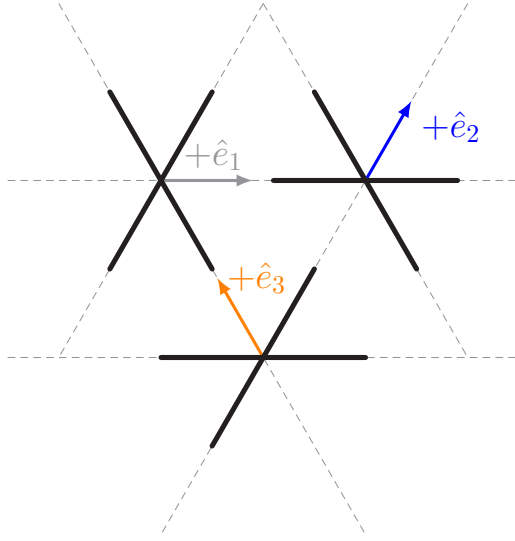


FIG. 2. Possible orientational states $\eta \equiv \hat{e}_k$, with $k = 1, 2, \text{ and } 3$. Bonding arms are represented by thick black lines and the generators of the triangular lattice \hat{e}_1 , \hat{e}_2 , and \hat{e}_3 are indicated by tiny coloured arrows. For this configuration no hydrogen bond is formed between these molecules.

done in Sec. IV for the Monte Carlo simulations. The comparison of the outcomes from both methods and our concluding remarks are presented in Sec. V.

II. MODEL

We study the symmetric version of the Henriques and Barbosa (H&B) [21] associating lattice gas (ALG) model, investigated in Refs. [22,34,35,41]. The model is defined on the triangular lattice (coordination number $z = 6$), where each site i can be either empty ($\sigma_i = 0$) or occupied by a single molecule ($\sigma_i = 1$). A chemical potential μ is associated to each particle in the system, since we will work in the grand canonical ensemble. Whenever two molecules occupy nearest-neighbor (NN) sites, they experience a repulsive “van der Waals” interaction, gaining an energy $\varepsilon > 0$. In addition, two NN molecules can form a hydrogen bond, which decreases their energy by a factor $-\gamma < 0$, provided that their bonding arms point toward each other. In fact, a key feature of the model analyzed here (and of other ALGs as well) is the existence of orientational degrees of freedom and related interactions introduced by bonding arms. In our case, each molecule has four bonding arms and two inert (nonbonding) arms, as shown in Fig. 2. The four bonding arms are all equivalent and always interact with those of NN molecules in the same manner, i.e., there is no distinction between donors and acceptors (of protons) here, in opposition to the original (nonsymmetric) H&B model [21]. The inert arms of a given molecule are in diametrically opposed lattice edges (forming an angle 180°), which results in three orientational states for each molecule (see Fig. 2). Following Ref. [41], we may conveniently define an orientational variable, η_i , pointing along one of the nonbonding directions of the molecule at site i . In this fashion, it is simply given by the generators of the triangular lattice, \hat{e}_k with $k = 1, 2$ and 3 , which are also depicted

in Fig. 2. Namely, $\eta_i \equiv \hat{e}_k$, where $\hat{e}_1 = \hat{i}$, $\hat{e}_2 = +\frac{1}{2}\hat{i} + \frac{\sqrt{3}}{2}\hat{j}$ and $\hat{e}_3 = -\frac{1}{2}\hat{i} + \frac{\sqrt{3}}{2}\hat{j}$.

With these definitions, we may write the Hamiltonian of this ALG model as

$$\mathcal{H}(\eta, \mathbf{r}) = \sum_{\langle i,j \rangle} \sigma_i \sigma_j [\varepsilon + u_{ij}] - \mu \sum_i \sigma_i, \quad (1)$$

where $\mathbf{r} = \mathbf{r}_i - \mathbf{r}_j$ is a unit vector in the set $\{\pm\hat{e}_1, \pm\hat{e}_2, \pm\hat{e}_3\}$. The second sum gives the total number of particles, N , while the first sum runs over all NN pairs (i, j) , whose orientational interaction is encoded in variable u_{ij} , given by [41]

$$u_{ij} = -\gamma \left(\frac{4}{3}\right)^2 [1 - (\eta_i \cdot \mathbf{r})^2][1 - (\eta_j \cdot \mathbf{r})^2]. \quad (2)$$

Note that whenever \mathbf{r} is parallel or antiparallel to η_i and/or η_j , molecules (i, j) do not form a hydrogen bond and $u_{i,j} = 0$; otherwise, $u_{i,j} = -\gamma$. Following most of the previous studies of the ALG model [22,34,35], we will use the parameter ε as the energy scale and set $\gamma/\varepsilon = 2$. In this way, the net interaction between two NN molecules forming (not forming) a hydrogen bond is attractive (repulsive). We therefore have as free parameters the dimensionless temperature $\bar{T} = k_B T/\varepsilon$ and chemical potential $\bar{\mu} = \mu/\varepsilon$. We remark that in Ref. [41] the temperature (called τ there) was defined in units of γ , so that $\tau = \bar{T}/2$.

As already discussed in the Introduction [Sec. I], from previous studies of the ALG model [22,34,35], one knows that its phase diagram exhibits three phases: disordered fluid (DF), low-density liquid (LDL), and high-density liquid (HDL). In the ground state ($\bar{T} = 0$), the DF phase has particle density $\rho = 0$ (the reason it is usually called GAS) and is the most stable phase for $\bar{\mu} < -2$. For $-2 < \bar{\mu} < 2$ the LDL phase is the one with the lowest free energy. In this phase, one of the four sublattices is empty while each of the other three is occupied by molecules in one of the orientational states, such that each molecule participates in four hydrogen bonds [see Fig. 3(a)]. Hence, the LDL phase has $\rho = 3/4$ and a fourfold degeneracy. For $\bar{\mu} > 2$ the HDL phase is the most stable, with the lattice fully occupied ($\rho = 1$) and all inert arms aligned along the same direction, as illustrated in Fig. 3(b). The HDL phase is threefold degenerate. It is quite simple to show that the DF-LDL and LDL-HDL phases coexist at $\bar{\mu} = -2$ and $\bar{\mu} = 2$, respectively, when $\bar{T} = 0$ [22,34].

III. TRANSFER-MATRIX ANALYSIS

A. Preliminaries

We define the transfer matrix, \tilde{M}_L , of the model on strips of infinite length and finite width L . As illustrated in Fig. 4, we consider square lattice strips with diagonal edges, with periodic boundary conditions in the finite (horizontal) direction. As usual, each possible state for a given row of the strip will be associated with a row and a column of \tilde{M}_L . Since each lattice site can be in four different states, we have a total of 4^L states for a strip of width L , so that \tilde{M}_L has dimension $4^L \times 4^L$. To investigate the full-occupancy case ($\bar{\mu} \rightarrow \infty$), where only three states are possible for each site, we can work with reduced matrices of dimension $3^L \times 3^L$. In any case, the element (i, j) of \tilde{M}_L is obtained by setting the row n in state i , the row $n + 1$

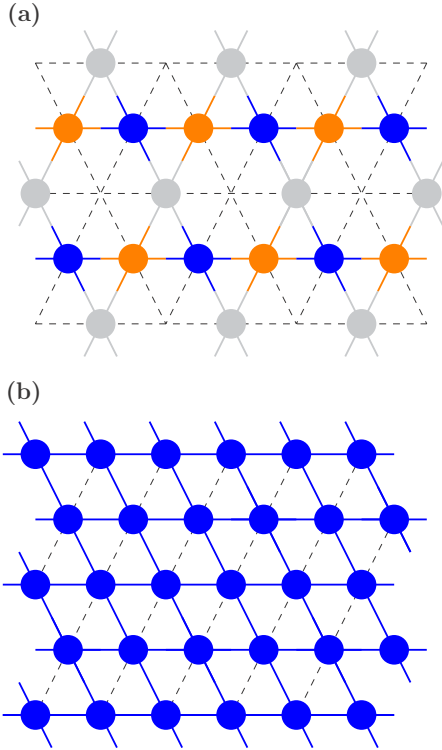


FIG. 3. Illustration of a ground state configuration of the (a) low-density liquid (LDL) phase and (b) high-density liquid (HDL) phase. Different colors represent molecules in distinct orientational states. The bonding arms are indicated by thick lines.

in state j and determining the statistical weight of this configuration. Then, $\tilde{M}_L(i, j) = \exp[(N_p \bar{\mu} + 2N_{hb} - N_{vdW})/2\tilde{T}]$, where N_p is the total number of particles on both rows (note that we are dividing this by 2), and N_{hb} and N_{vdW} counts the *effective* number of hydrogen bonds and van der Waals interactions (i.e., first neighbors) in these rows, respectively. By “effective,” we mean that we are counting once (twice) interactions along the horizontal (diagonal and vertical) direction and, then, dividing them by 2. In this way, the “internal” interactions, along the vertical and diagonal directions, are counted once, while each one in the horizontal contribute with 1/2 in each state, since they appear in two states.

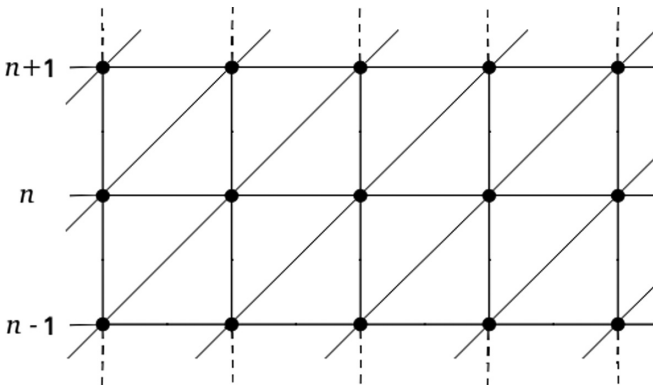


FIG. 4. Illustration of the approach to the triangular lattice used in our transfer-matrix calculations. A strip of width $L = 5$ is shown.

It is hard to deal directly with \tilde{M}_L , because all of its elements are nonnull. Therefore, to save computer RAM memory and speed up the calculations, we replace the procedure of adding an entire row, by the procedure of adding a single elementary cell (formed by squares with a diagonal edge). Working in this way, we have to deal with $L + 1$ matrices, $\tilde{T}_L^{(s)}$, so that $\tilde{M}_L = \tilde{T}_L^{(L)} \cdot \tilde{T}_L^{(L-1)} \dots \tilde{T}_L^{(0)}$. Here, $\tilde{T}_L^{(0)}$ creates a new site in row $n + 1$ above a complete row n ; the matrices $\tilde{T}_L^{(s)}$, with $1 \leq s \leq L - 1$, add new elementary cells to row $n + 1$; and finally $\tilde{T}_L^{(L)}$ completes the row $n + 1$ by imposing the appropriated (periodic here) boundary conditions (see, e.g., Refs. [43,44] for more details). The advantage of this method relies on the fact that the matrices $\tilde{T}_L^{(s)}$ are very sparse. In fact, the total number of nonnull terms summing over all matrices $\tilde{T}_L^{(s)}$ is only $(16L - 8)4^L$.

If $\Lambda_L^{(k)}$ denotes the eigenvalues of \tilde{M}_L , for given values of $\bar{\mu}$ and \tilde{T} , with $\Lambda_L^{(0)} > |\Lambda_L^{(1)}| > |\Lambda_L^{(2)}| > \dots$, then the (dimensionless) negative free energy density is

$$f(L) = \frac{\zeta}{L} \ln \Lambda_L^{(0)}, \quad (3)$$

where ζ is a geometric factor given by the thickness of the added row when its circumference is L , which in our case is $\zeta = 2/\sqrt{3}$. The correlation length $\xi_k(L)$ associated with the k th subleading eigenvalue is given by

$$\xi_k^{-1}(L) = \zeta \ln \frac{\Lambda_L^{(0)}}{|\Lambda_L^{(k)}|}. \quad (4)$$

From these correlation lengths, we may defined the scaled gaps $X_k(L) = L/[2\pi\xi_k(L)]$. Note that all these quantities obviously depend also on $\bar{\mu}$ and \tilde{T} . Close to a critical point (\tilde{T}_c or $\bar{\mu}_c$), from finite-size scaling [45], we expect that

$$X_k(L; \tilde{T}, \bar{\mu}) = X_k^* + a_i t L^{y_i} + a_1 L^{y_1} + a_2 L^{y_2} + \dots, \quad (5)$$

where $y_i > 0$ is the temperature exponent, $y_i < 0$ ($i = 1, 2, \dots$) are irrelevant exponents, and $t = \tilde{T} - \tilde{T}_c$ if $\bar{\mu}$ is kept fixed or $t = \bar{\mu} - \bar{\mu}_c$ when \tilde{T} is the fixed parameter.

In conformally invariant systems, the critical free energy density is expected to follow

$$f(L) = f_\infty + \frac{\pi c}{6L^2} + p_1 L^{z_1} + \dots, \quad (6)$$

where c is the conformal anomaly [46] and z_1 is a negative exponent.

B. The full-occupancy limit

Let us start analyzing the limiting case $\bar{\mu} \rightarrow \infty$, where all lattice sites are occupied by molecules. Here, we can work with smaller transfer matrices, as noticed above, which allows us to investigate strip widths up to $L = 16$. As recently demonstrated by some of us, in such a limit the system displays only the DF and HDL phases, separated by a critical point in the class of the 2D 3-state Potts model [41].

If a critical point exists at some critical temperature \tilde{T}_c^* , from Eq. (5), then one may expect that curves of the scaled gaps $X_k(L - \ell; \tilde{T})$ and $X_k(L + \ell; \tilde{T})$ versus \tilde{T} (e.g., with $\ell = 1$) cross at pseudocritical temperatures $\tilde{T}_{c,k}(L)$, which shall converge to \tilde{T}_c^* as $L \rightarrow \infty$. Therefore, $\tilde{T}_{c,k}(L)$ can be determined from the condition $X_k(L - 1, \tilde{T}_{c,k}) = X_k(L + 1, \tilde{T}_{c,k}) \equiv$

TABLE I. Finite-size estimates of the pseudocritical temperature $\bar{T}_{c,k}$ and scaling dimension $X_{c,k}$ from the condition $X_k(L - 1, \bar{T}_{c,k}) = X_k(L + 1, \bar{T}_{c,k})$ for $k = 1$ (left) and $k = 2$ (right). The central charges $c^{(k)}$, calculated at $\bar{T}_{c,k}(L)$, are also shown.

| L | $\bar{T}_{c,1}$ | $X_{c,1}$ | $c^{(1)}$ | $\bar{T}_{c,2}$ | $X_{c,2}$ | $c^{(2)}$ |
|-----|-----------------|--------------|--------------|-----------------|--------------|--------------|
| 3 | 0.9630812528 | 0.1153561805 | 0.9439481004 | 0.9831360600 | 0.1951137102 | 0.9400187288 |
| 4 | 0.9581778321 | 0.1122361525 | 0.9019637901 | 0.9689256192 | 0.1810700192 | 0.8996045252 |
| 5 | 0.9546313471 | 0.1090076877 | 0.8651449784 | 0.9611962232 | 0.1708572156 | 0.8639745823 |
| 6 | 0.9530663416 | 0.1071998513 | 0.8438815963 | 0.9575263053 | 0.1648349316 | 0.8433113197 |
| 7 | 0.9524498263 | 0.1063326346 | 0.8322698047 | 0.9557272984 | 0.1612950160 | 0.8319934887 |
| 8 | 0.9522229606 | 0.1059533630 | 0.8256760684 | 0.9547690621 | 0.1590849673 | 0.8255533747 |
| 9 | 0.9521529738 | 0.1058159572 | 0.8216678338 | 0.9542109914 | 0.1576018062 | 0.8216323836 |
| 10 | 0.9521470966 | 0.1058006641 | 0.8190595772 | 0.9538600720 | 0.1565417468 | 0.8190774634 |
| 11 | 0.9521675217 | 0.1058493262 | 0.8172623591 | 0.9536256433 | 0.1557459461 | 0.8173147797 |
| 12 | 0.9521981542 | 0.1059325169 | 0.8159665891 | 0.9534614919 | 0.1551257762 | 0.8160423453 |
| 13 | 0.9522318614 | 0.1060345131 | 0.8149983146 | 0.9533421966 | 0.1546283056 | 0.8150903408 |
| 14 | 0.9522654200 | 0.1061464695 | 0.8142535202 | 0.9532528474 | 0.1542199764 | 0.8143571526 |
| 15 | 0.9522974007 | 0.1062632003 | 0.8136666597 | 0.9531842311 | 0.1538784508 | 0.8137787074 |

$X_{c,k}(L)$, from which a pseudocritical estimate [$X_{c,k}(L)$] of the asymptotic scaling dimension X_k^* is also obtained. The values of these quantities for $k = 1$ and $k = 2$ are shown in Table I. The first thing to note there is that $\bar{T}_{c,1}$ has a nonmonotonic behavior, initially decreasing and then increasing with L . This prevents any reliable extrapolation of this temperature. The convergence of $\bar{T}_{c,2}$, however, is monotonic and, so, we will focus on it to estimate \bar{T}_c^* .

In general, from finite-size scaling, one expects that

$$\bar{T}_{c,k}(L) = \bar{T}_c^* + b_1 L^{-\omega_1} + b_2 L^{-\omega_2} + \dots, \quad (7)$$

whose exponents are related to those in Eq. (5) as $\omega_1 = y_t - y_1$ and $\omega_2 = y_t - y_2$. Then, by considering $b_i = 0$ for $i \geq 2$ and performing three-point (3-pt) extrapolations of the values of $\bar{T}_{c,2}$ in Table I [with \bar{T}_c^* , b_1 and ω_1 as unknowns in Eq. (7)], we find the temperatures displayed in Table II. Note that for the largest L 's they are varying at the fifth decimal place. A second round of 3-pt extrapolations (now of the extrapolated values in Table II) yields $0.952806 \leq \bar{T}_c^* \leq 0.952818$, for the four largest sets of widths, without any clear tendency to increase or decrease. Hence, this gives $\bar{T}_c^* = 0.952812(6)$.

TABLE II. Extrapolated temperatures, \bar{T}_c^* , and corresponding correction exponents, ω_1 , from 3-pt extrapolations of the values of $\bar{T}_{c,2}$ displayed in Table I, considering Eq. (7) and sets of sizes $(L - 1, L, L + 1)$. The resulting central charges, c , from analogous extrapolations of the values of $c^{(2)}$ in Table I are also shown.

| L | \bar{T}_c^* | ω_1 | c |
|-----|---------------|------------|-----------|
| 4 | 0.9397502 | 1.3793263 | - |
| 5 | 0.9516285 | 2.6536683 | 0.7857046 |
| 6 | 0.9529237 | 3.2158880 | 0.8086578 |
| 7 | 0.9530776 | 3.3614896 | 0.8119752 |
| 8 | 0.9530316 | 3.2893957 | 0.8121525 |
| 9 | 0.9529681 | 3.1489286 | 0.8117281 |
| 10 | 0.9529211 | 3.0137856 | 0.8112940 |
| 11 | 0.9528904 | 2.9040695 | 0.8109670 |
| 12 | 0.9528705 | 2.8173407 | 0.8107358 |
| 13 | 0.9528570 | 2.7468393 | 0.8105667 |
| 14 | 0.9528474 | 2.6875514 | 0.8104331 |

This value differs by only 0.02% from the one estimated from MC simulations in Ref. [41]: $\bar{T}_c^* \approx 0.9526$.

The resulting exponents ω_1 from the first 3-pt extrapolations are also displayed in Table II. Three-point extrapolations of them, assuming again a power-law correction, return values close (and converging toward) to $\omega_1 = 2$ for the largest sets of widths. We remark that, according to Queiroz [47], the irrelevant exponents in Eq. (5) are given by $y_1 = -4/5$ and $y_2 = -8/5$ for the three-state Potts model, whose critical thermal exponent is $y_t = 6/5$. This means that $\omega_1 = 2$ and $\omega_2 = 14/5 = 2.8$ in this case. By assuming that $\omega_1 = 2$ and $b_i = 0$, for $i \geq 3$ in Eq. (7), we estimate the exponents ω_2 for different L 's from 4-pt extrapolations; and subsequent 3-pt extrapolations of them yield values close to $14/5$ for the largest L 's. So, the correction exponents of the ALG model in the full lattice regime are consistent with the ones for the 3-state Potts model.

The finite-size amplitudes $X_{c,1}$ and $X_{c,2}$ in Table I, however, do not agree with the ones expected for the 2D 3-state Potts class. In fact, for conformally invariant models in this class, the asymptotic values of these quantities are $X_1^* = 2 - y_h = 2/15$ and $X_2^* = 2 - y_t = 4/5$. However, our values of $X_{c,1}$ for the largest L 's are $\sim 20\%$ smaller than $2/15$, though they display a nonmonotonic convergence and are increasing for large L 's. So, it may be the case that for very large strip widths they will attain the expected Potts value. For $X_{c,2}$, our values are smaller than $4/5$ by a factor ~ 5 and are still decreasing, without any indication of changing in this behavior. Actually, the values in Table I extrapolate to $X_2^* \approx 0.15$, suggesting that $y_t \approx 1.85$ and then $\nu = 1/y_t \approx 0.54$. Thereby, we can be either dealing with a system displaying very slow convergences in these quantities (what seems strange in the case of $X_{c,2}$) or the ALG is not a conformally invariant model or it belongs to a different universality class.

The central charge is somewhat consistent with the 3-state Potts class, for which $c = 4/5$. In fact, the values of c , calculated as $c(L) = 3[f(L - 1) - f(L + 1)](L - 1)^2(L + 1)^2/2\pi L$ at the pseudocritical temperatures $\bar{T}_{c,1}$ and $\bar{T}_{c,2}$, are shown in Table I; and they approximate $4/5$ as the system size increases. However, 3-pt extrapolations of such estimates (assuming power-law corrections) return $c \gtrsim 0.81$ (see Table II).

TABLE III. Critical free energies, f , and scaled gaps X_1 and X_2 calculated at the critical temperature $\bar{T}_c^* = 0.952812$. The central charges, c , estimated from these free energies are also shown.

| L | f | X_1 | X_2 | c |
|-----|----------|----------|----------|----------|
| 2 | 5.029729 | 0.112107 | 0.180682 | – |
| 3 | 4.960323 | 0.109445 | 0.168819 | 0.944204 |
| 4 | 4.937032 | 0.107661 | 0.161966 | 0.902030 |
| 5 | 4.926737 | 0.106952 | 0.158348 | 0.865111 |
| 6 | 4.921304 | 0.106774 | 0.156322 | 0.843869 |
| 7 | 4.918080 | 0.106823 | 0.155076 | 0.832298 |
| 8 | 4.916008 | 0.106965 | 0.154240 | 0.825738 |
| 9 | 4.914595 | 0.107143 | 0.153641 | 0.821754 |
| 10 | 4.913587 | 0.107334 | 0.153189 | 0.819162 |
| 11 | 4.912844 | 0.107525 | 0.152836 | 0.817377 |
| 12 | 4.912280 | 0.107713 | 0.152551 | 0.816090 |
| 13 | 4.911841 | 0.107895 | 0.152317 | 0.815052 |
| 14 | 4.911494 | 0.108069 | 0.152121 | 0.814293 |
| 15 | 4.911213 | 0.108237 | 0.151953 | 0.813804 |
| 16 | 4.910984 | 0.108397 | 0.151809 | – |

Further 3-pt extrapolations of the extrapolated values in Table II, considering the largest L 's available, do not improve this, once they yield $c \approx 0.809$, which differs by $\sim 1\%$ from the Potts value.

Table III shows the scaled gaps X_1 and X_2 calculated at the critical point $\bar{T}_c^* = 0.952812$. However, these quantities are very similar to those in Table I, obtained at the pseudocritical temperatures. The critical free energies at $\bar{T}_c^* = 0.952812$, as well as the central charges obtained from them (calculated as indicated above) are also depicted in Table III. Once again, the values of c present an appreciable difference from $c = 4/5$ and extrapolations of them have deviations similar to those observed above.

C. The DF-HDL transition line

Employing the same analysis from the previous subsection, but for finite $\bar{\mu}$, we find that the critical DF-HDL transition extends to chemical potentials down to $\bar{\mu} \sim 2$, giving rise to a DF-HDL transition line, as found in the mean-field solutions of the model on Husimi lattices [34,41]. Given the nonmonotonic convergence observed above in the pseudocritical points estimated from X_1 , we will focus here only on those calculated from X_2 . The pseudocritical transition lines obtained from the condition $X_2(L-1, \bar{T}_c^*) = X_2(L+1, \bar{T}_c^*)$, for fixed values of $\bar{\mu}$, are shown in Fig. 5(a), for $L \leq 11$. (Here, it is quite hard to go beyond $L = 12$, once the TMs have $4^L \times 4^L$ terms. Actually, most of our results will be limited to $L \leq 10$.) It is important to notice that such lines never cross each other, indicating that the DF-HDL transition is always continuous.

Three-point extrapolations of the pseudocritical lines—assuming the finite-size correction of Eq. (7) for fixed $\bar{\mu}$, with $b_i = 0$ for $i > 1$, and considering the sets of widths (5,7,9) and (7,9,11)—yield lines whose values of \bar{T}_c^* always differ by less than 0.2%. This corresponds to differences (and error bars) at most at the third decimal place, which is accurate enough for our purposes.

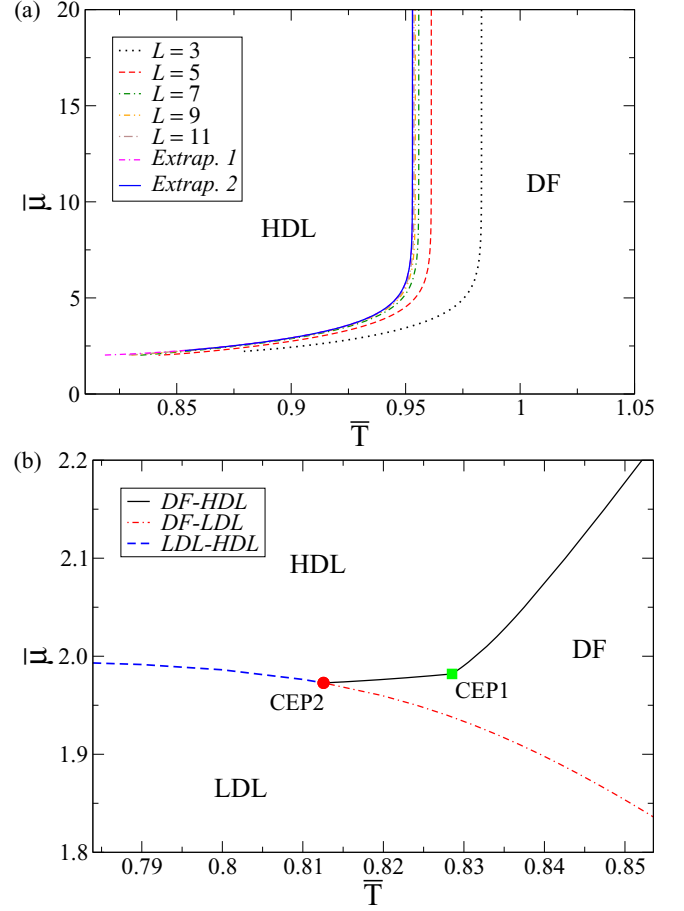


FIG. 5. (a) Pseudocritical lines separating the DF and HDL phases, obtained from $X_2(L-1, \bar{T}_c^*) = X_2(L+1, \bar{T}_c^*)$ for fixed values of $\bar{\mu}$, for the indicated L 's. The outcomes from 3-pt extrapolations of these lines considering the sets (5,7,9) (Extrap. 1) and (7,9,11) (Extrap. 2) are also shown. (b) Detail of the region where the DF-HDL, DF-LDL, and LDL-HDL transition lines, for $L = 7$, meet. The green square and the red circle indicate the two estimates for the critical-end-point.

Interestingly, the pseudocritical lines have a corner at $\bar{\mu} \approx 2$, which may be seen as their end-point. An example of this is shown in Fig. 5(b), in the line for $L = 7$. As it will be demonstrated below, the critical DF-HDL line ends at a critical end-point (CEP). The coordinates $(\bar{T}_{\text{cep},1}, \bar{\mu}_{\text{cep},1})$ of the CEP, assuming that it is located at the corner, are depicted in Table IV. Since the DF-HDL transition lines continue below these corners and finally meet the DF-LDL and LDL-HDL

TABLE IV. Estimates for the critical-end-point from the corner in the DF-HDL transition lines (leftmost values) and from the point where such lines meet the other transition lines (rightmost values).

| L | $\bar{T}_{\text{cep},1}$ | $\bar{\mu}_{\text{cep},1}$ | $\bar{T}_{\text{cep},2}$ | $\bar{\mu}_{\text{cep},2}$ |
|-----|--------------------------|----------------------------|--------------------------|----------------------------|
| 3 | 0.884217 | 2.264032 | 0.801210 | 2.010048 |
| 5 | 0.841799 | 2.018722 | 0.812741 | 1.982581 |
| 7 | 0.828528 | 1.981947 | 0.812563 | 1.972774 |
| 9 | 0.823467 | 1.970668 | 0.812692 | 1.968213 |

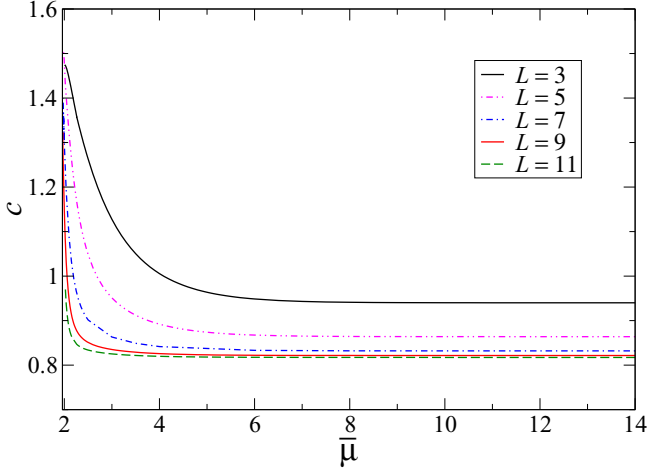


FIG. 6. Central charge c versus $\bar{\mu}$ calculated at the pseudocritical transition lines from Fig. 5(a), for the indicated widths.

transition lines [see Fig. 5(b)], one obtains another set of estimates ($\bar{T}_{\text{cep},2}$, $\bar{\mu}_{\text{cep},2}$) for the CEP. As shows Table IV, in this last case the temperatures oscillate around $\bar{T}_{\text{cep},2} = 0.81266$ (considering the three largest L 's). The temperatures of the corners seem to converge toward this value as L increases; though a 3-pt extrapolation of them [following Eq. (7), considering the largest L 's] returns a slightly larger value: $\bar{T}_{\text{cep},1} = 0.81681$. This deviation, of $\sim 0.5\%$, is certainly due to the small widths considered here, so that it is reasonable to regard $\bar{T}_{\text{cep}} = 0.815(3)$ as our estimate for the CEP temperature. This value is close, but a bit smaller than $\bar{T}_{c/\text{tc}} = 0.825$, which was found in previous MC simulations of the ALG model and reported as a critical point in Ref. [22] and as a tricritical point in Ref. [35]. Our estimate is also smaller than the value found for the triple point ($\bar{T}_{\text{tp}} = 0.835$) in the Husimi lattice solution of the model [34].

The 3-pt extrapolations of the values of $\bar{\mu}_{\text{cep},1}(L)$ and $\bar{\mu}_{\text{cep},2}(L)$ for the largest L 's, assuming power-law corrections similarly to Eq. (7), yield $\bar{\mu}_{\text{cep},1} = 1.9589$ and $\bar{\mu}_{\text{cep},2} = 1.9605$, respectively, indicating that $\bar{\mu}_{\text{cep}} = 1.9597(8)$. This result agrees with the mean-field value found in Ref. [34] for the triple point ($\bar{\mu}_{\text{tp}} = 1.959$) and differs by $\approx 3\%$ from the critical point reported in Ref. [22] ($\bar{\mu}_c = 2.02$).

The central charges calculated along the pseudocritical transition lines from Fig. 5(a) are shown in Fig. 6 as a function of $\bar{\mu}$. We may note that $c(L)$ is almost independent of the chemical potential for $\bar{\mu}_c \gtrsim 10$ (similarly to \bar{T}_c), having values very close to those of $c^{(2)}$ in Table I for $\bar{\mu} \rightarrow \infty$. When $\bar{\mu}$ approximates $\bar{\mu}_{\text{cep}}$, however, one sees that c passes to increase and to display stronger finite-size corrections. The larger L , the closer the approximately constant part of the lines get to $\bar{\mu}_{\text{cep}}$ before deviating upward. This strongly suggests that for very large L 's one must have $c \approx 0.8$ in the entire DF-HDL line, indicating that it belongs to the 3-state Potts class.

D. The LDL-HDL transition line

The LDL-HDL transition is the only one for which all previous studies of the ALG model agree; the phases are separated by a coexistence line, which exists in a narrow

chemical potential interval near $\bar{\mu} = 2$ [22,34,35]. Therefore, in this case, it is convenient to determine the transition lines by varying $\bar{\mu}$ for fixed values of \bar{T} . For the strip widths analyzed here, crossings in the curves of $X_k(L; \bar{\mu})$ versus $\bar{\mu}$ for different L 's are only observed for $k \geq 3$. The curves of $X_1(L; \bar{\mu})$ and $X_2(L; \bar{\mu})$ only exhibit a maximum in the coexistence region. The transition lines obtained from the condition $X_3(L-1, \bar{\mu}_c) = X_3(L+1, \bar{\mu}_c)$ are depicted in Fig. 7(a). The lines for the smallest widths present maxima in the region close to the CEP, which are absent in those for the largest L 's. This turns the extrapolation of these lines unreliable in this region, which is the most important part of such curves, since they are always very close to $\bar{\mu} = 2$ for low temperatures.

Motivated by this and also to confirm the first-order nature of the LDL-HDL transition, we obtain an alternative estimate for the LDL-HDL transition line through the correlation length $\xi_k^{-1}(L)$, defined in Eq. (4), for $k = 6$. We remark that, given the fourfold (threefold) degeneracy of the ground state of the LDL (HDL) phase, a total of seven possible phases (divided into two sets with three and four equivalent ones) coexist at the LDL-HDL transition line. This means that the seven largest eigenvalues (from Λ_0 to Λ_6) of the TMs shall be degenerated in the thermodynamic limit ($L \rightarrow \infty$). Hence, curves of $\xi_6^{-1}(L)$ versus $\bar{\mu}$, for a given \bar{T} , are expected to display a minimum at the coexistence [48–51]. As exemplified in Fig. 7(b) for $\bar{T} = 0.75$, such behavior is indeed found in these curves, confirming that this is a discontinuous transition. The coexistence lines estimated from the loci of these minima are depicted in Fig. 7(c). It is noteworthy that $\bar{\mu}_c(\bar{T})$ decreases with L in Fig. 7(a), while for these last estimates an increasing behavior is observed in Fig. 7(c).

To extrapolate these lines, we recall that finite-size scaling predicts exponential corrections at the coexistence [45], such that

$$\bar{\mu}_c(L) = \bar{\mu}_c^* + ae^{-bL} + \dots, \quad (8)$$

for a given \bar{T} . For a 3-pt extrapolation this gives $\bar{\mu}_c^* = \frac{\bar{\mu}_c(L+1)\bar{\mu}_c(L-1) - \bar{\mu}_c(L)^2}{\bar{\mu}_c(L+1) + \bar{\mu}_c(L-1) - 2\bar{\mu}_c(L)}$. The resulting curve from such a extrapolation, for the three largest L 's, is shown in Fig. 7(c).

E. The DF-LDL transition line

The transition lines separating the disordered and LDL phases were estimated following the same procedures from the previous subsection, but varying \bar{T} for fixed values of $\bar{\mu}$. The curves obtained from the condition $X_1(L-1, \bar{T}_c) = X_1(L+1, \bar{T}_c)$ are depicted in Fig. 8(a), where one sees that \bar{T}_c , for a given $\bar{\mu}$ decreases with L . Significantly, these lines never cross each other, indicating that no tricritical point exists in the DF-LDL transition, in contrast with the result from MC simulations reported in Ref. [35]. Since one knows that this transition is discontinuous at $\bar{T} = 0$, and for low \bar{T} as well, the absence of the tricritical point implies that the entire transition line is of first-order nature, in agreement with the Husimi lattice solution of the model [34].

Additional evidence of this is obtained from the curves of ξ_4^{-1} versus \bar{T} , for a given $\bar{\mu}$, which have minima hallmarking the coexistence. A behavior analogous to that seen in Fig. 7(b) for ξ_6^{-1} at the LDL-HDL transition. Note that in the case of

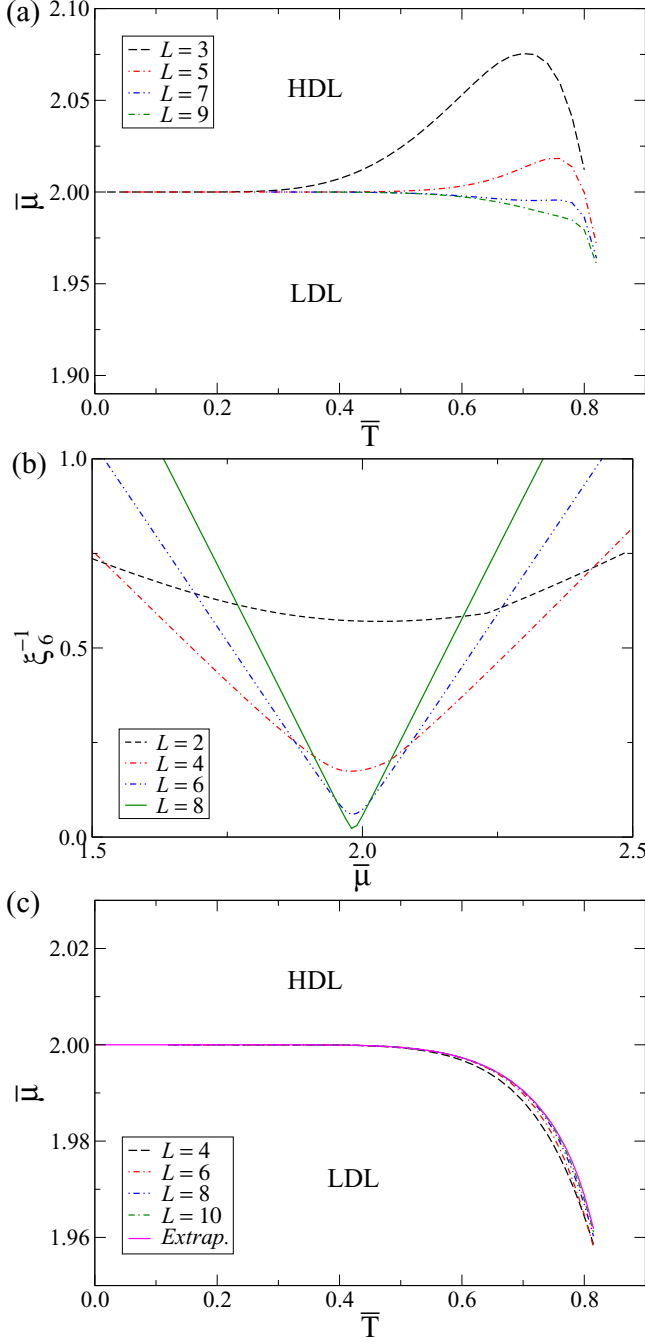


FIG. 7. (a) Estimates of the LDL-HDL coexistence line from the condition $X_3(L-1, \bar{\mu}_c) = X_3(L+1, \bar{\mu}_c)$ for fixed values of \bar{T} , for the indicated L 's. (b) Inverse correlation length ξ_6^{-1} versus $\bar{\mu}$ for $\bar{T} = 0.75$ and the indicated L 's. (c) LDL-HDL coexistence lines obtained from the minima in the curves in panel (b) and similarly ones for other temperatures. The extrapolated curve (Extrap.), from a 3-pt extrapolation following Eq. (8), is also shown.

the DF phase (one ground state) coexisting with the LDL phase (which has four equivalent ground states), minima are indeed expected in ξ_4^{-1} . From such minima, we estimate the coexistence lines displayed in Fig. 8(b). Interestingly, in this case the values of $\bar{T}_c(\bar{\mu})$ increases with L , in opposition to the behavior seen in Fig. 8(a).

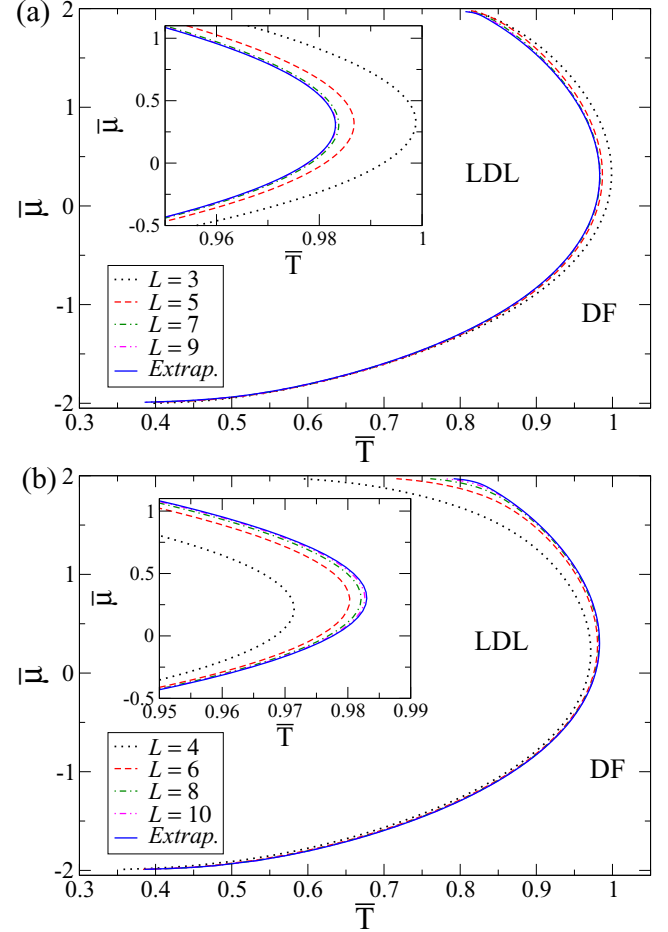


FIG. 8. Finite-size estimates of the DF-LDL coexistence line: (a) from the condition $X_1(L-1, \bar{T}_c) = X_1(L+1, \bar{T}_c)$, for fixed values of $\bar{\mu}$; and (b) from the minima in the inverse correlation length ξ_4^{-1} . The respective extrapolated curves (Extrap.), from a 3-pt extrapolation following Eq. (8), are shown in both panels.

Figures 8(a) and 8(b) present also the asymptotic curves, obtained from 3-pt extrapolations assuming exponential finite-size corrections in $\bar{T}_c(L)$ similarly to Eq. (8) [i.e., $\bar{T}_c(L) \simeq \bar{T}_c^* + ae^{-bL}$]. The difference between the values of $\bar{T}_c^*(\bar{\mu})$ along these lines is always smaller than 0.5% and in the main part of them it is $\lesssim 0.01\%$. The turning point in the coexistence line (i.e., the point where \bar{T}_c^* is maximum) is located at $\bar{T}_c^* \approx 0.983$ and $\bar{\mu}_c^* \approx 0.31$.

The complete phase diagram, presenting all the transition lines found in our MT calculations, will be presented in Sec. V, where they are compared with the results from the MC simulations discussed in the next section.

IV. MONTE CARLO SIMULATIONS

A. Simulation details and quantities of interest

The thermodynamic properties of the symmetric ALG model were also obtained via extensive Monte Carlo (MC) simulation on the triangular lattice with periodic boundary conditions. We study system sizes $L = 32, 48, 64, 96, 128$

and 192 using the standard Metropolis algorithm in the grand canonical ensemble.

Following references [22,35], simulations with fixed chemical potential are used to locate the DF-HDL line while simulations along isotherms in the $\bar{\mu}$ - \bar{T} plane are used to locate the DF-LDL and LDL-HDL coexistence lines. We study $\bar{\mu} = 1.95, 2.3, 2.4, 2.5, 2.6, 5.0$, and 10 in the HDL region and use a temperature interval $0.50 \leq \bar{T} \leq 0.97$ in the LDL region.

Studies of the HDL region are performed in two steps. First, broad ranges of temperature are studied to identify the region of peaks in the response functions. In this step 50 independent realizations are used to compute averages. After identifying the region of interest for each system size, additional simulations are performed in a reduced range of temperatures. The number of points around the maximum depends on the system size; for $L = 64, 128$ we use 60 points while for larger system sizes 30 points are sufficient. In this step 100 independent replicas are used. In all simulations we use 10^6 MC steps for equilibration, followed by $10^5 - 2 \times 10^6$ MC steps for data production.

The transition between the HDL and the DF phases can be analyzed using the order parameters [39,41],

$$\theta(\bar{T}, \bar{\mu}; L) \equiv \frac{3}{2} \left[\frac{\max(n_1, n_2, n_3)}{N} - \frac{1}{3} \right] \quad (9)$$

and

$$Q(\bar{T}, \bar{\mu}; L) \equiv \frac{1}{N} \sqrt{n_1^2 + n_2^2 + n_3^2 - n_1 n_2 - n_1 n_3 - n_2 n_3}, \quad (10)$$

where n_k denotes the number of molecules in orientational state k and $N = \sum_{k=1}^3 n_k$ is the total number of molecules. In the DF phase, one has $n_1 \approx n_2 \approx n_3$, so that $\theta \rightarrow 0$ and $Q \rightarrow 0$. However, $\theta \rightarrow 1$ and $Q \rightarrow 1$ in the HDL phase, where, e.g., $n_1 \approx N$ and $n_2 \approx n_3 \approx 0$.

To analyze the transitions we also use the susceptibilities related to the order parameters,

$$\chi_X(\bar{T}; L) = \frac{L^2}{\bar{T}} [\langle X^2 \rangle - \langle X \rangle^2], \quad (11)$$

with $X = \theta$ or Q ; the specific heat at constant volume [52]

$$c_V(\bar{T}; L) = \frac{1}{V\bar{T}^2} \left[\langle E^2 \rangle - \langle E \rangle^2 - \frac{(\langle EN \rangle - \langle E \rangle \langle N \rangle)^2}{\langle N^2 \rangle - \langle N \rangle^2} \right] \quad (12)$$

and the isothermal compressibility

$$\kappa(\bar{T}; L) = \frac{V}{k_B \bar{T}} \left(\frac{\langle N^2 \rangle - \langle N \rangle^2}{\langle N \rangle^2} \right). \quad (13)$$

In Eqs. (11)–(13), $\langle \cdot \rangle$ denotes grand canonical averages.

B. Discontinuous transitions

In this subsection we present the results for DF-LDL and LDL-HDL transitions. As reported in the Refs. [22,35] the density plays the role of an order parameter for the referred transitions. Figures 9(a) and 9(b) show the density as a function of chemical potential for the DF-LDL transition and the LDL-HDL transition, respectively. The density histograms

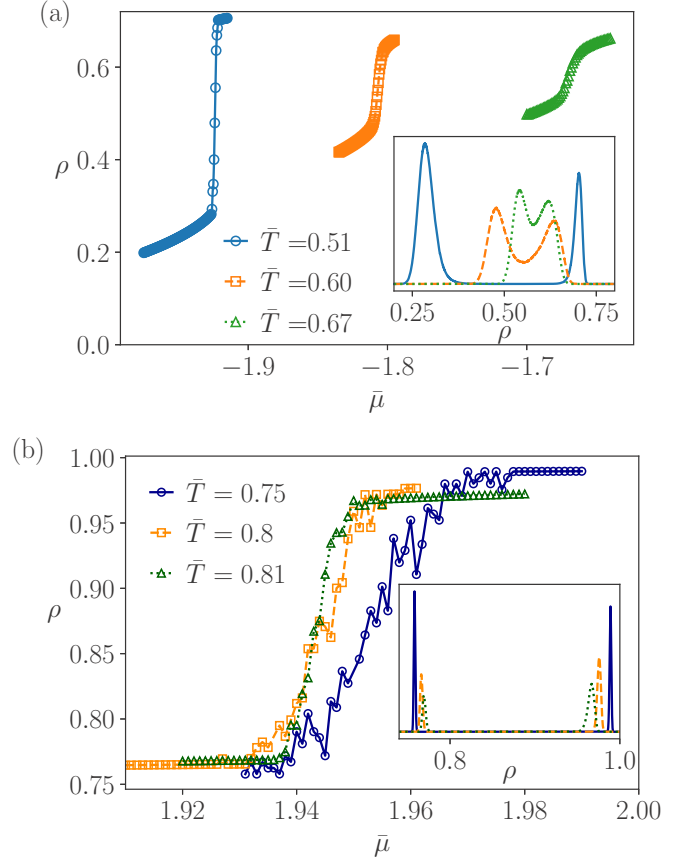


FIG. 9. Density versus chemical potential for distinct temperatures, as indicated, at DF-LDL (a) and LDL-HDL (b) transitions. Insets show histograms of the density near the DF-LDL and LDL-HDL coexistence. The system size is $L = 64$ in panel (a) and $L = 128$ in panel (b).

for each transition are shown in the insets of Figs. 9(a) and 9(b). In both cases, the histograms are bimodal indicating a discontinuous transition and confirming the results from the transfer matrix (TM) calculations (see Secs. III D and III E). For each temperature, we plotted the histogram for the chemical potential that was closest to the coexistence value within our resolution ($\Delta\bar{\mu} = 10^{-4}$ or larger). We take the coexistence chemical potential as that for which the heights of the two peaks are equal.

The coexistence chemical potential is estimated as follows: First we identify the values of the maxima of the probability distributions, $\max[P(\rho_{DF})]$ and $\max[P(\rho_{LDL})]$, for each chemical potential studied (see blue crosses and red pluses in Fig. 10). Subsequently, we plot the $\max[P(\rho_{LDL,DF})]$ as function of chemical potential as shown in Fig. 10 for $\bar{T} = 0.55$. The crossing point of the curves is estimated through a polynomial fit in the vicinity of the intersection, using the reciprocals of the variance ($1/\sigma_i^2$) of the averages computed over the replicas as weights for the polynomial fit of the points. In most cases, 7 points around the intersection region are enough to obtain a satisfactory region of crossing. The order of the polynomial is chosen as the lowest order that yields random behavior of residuals; a third-order polynomial fit was sufficient in most cases. Subsequently, the error of the

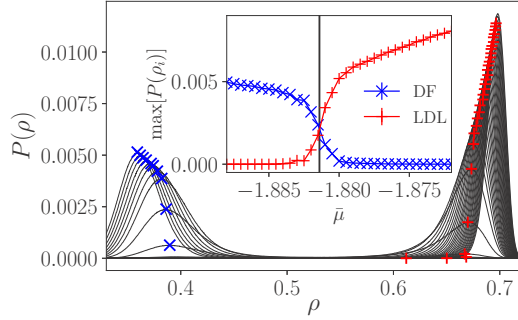


FIG. 10. Main panel: thin black lines represent the probability distribution of the density ρ for distinct chemical potentials and $\bar{T} = 0.55$. Blue (red) crosses (pluses) indicate the location of the maximum of probability distributions in the DF (LDL) phase. Inset: maxima of the probability distributions for the disordered phase (blue crosses) and the LDL phase (red pluses) versus chemical potential $\bar{\mu}$. The vertical line indicates the crossing point. The system size is $L = 64$.

fit was computed through the root-mean-square error (RMSE) over the points used in the fit. Finally, the uncertainty in the crossing-point estimate is computed as the square root of the RMSE resulting from each polynomial. This procedure yields the dots in the phase diagram of Fig. 15.

In the region around $\bar{\mu} = 0$, $\bar{T} > 0.95$ the densities ρ_{LDL} and ρ_{DF} are very similar and the coexistence temperature and chemical potential cannot be obtained using the density histogram [see Fig. 15(b)].

For the LDL-HDL transition, the data for the density are very noisy for $\bar{T} \leq 0.75$ [see Fig. 9(b)] and it is not possible to use the procedure described above to determine the coexistence chemical potential. For these cases, we adopted the following procedure: for each point on the curve $\max[P(\rho_i)] \times \bar{\mu}$ (see inset of Fig. 10) we sum a Gaussian random variable proportional to the error bar of that point. We then fit the curves and estimate the crossing point. An average is computed over 10^4 realizations of this procedure and the error is propagated as described above. The values obtained using this strategy are the triangles in Fig. 15 and are in good agreement with the TM results of Sec. III D.

The highest temperature for which we observe LDL-HDL coexistence is $\bar{T} = 0.816$, $\bar{\mu} = 1.9498(7)$, for the next

temperature studied, $\bar{T} = 0.817$, we observe LDL-DF coexistence and then a continuous DF-HDL transition. We therefore take this \bar{T} , $\bar{\mu}$ pair as an estimate of the critical end point (CEP) at which the LDL-HDL line meets the DF-HDL and the DF-LDL lines (see Sec. III C). This value, $\bar{T}_{\text{cep}} = 0.816$, $\bar{\mu}_{\text{cep}} = 1.9498(7)$, is in excellent agreement with the estimate from TM calculations, $\bar{T}_{\text{cep, TM}} = 0.815(1)$, $\bar{\mu}_{\text{cep, TM}} = 1.9597(8)$. Our estimate for $\bar{T}_{\text{cep, MC}}$ and $\bar{\mu}_{\text{cep, MC}}$ is smaller than the values reported in previous MC simulations [22,35] for c_2 and tc_2 (see Fig. 1).

C. Continuous transitions

To determine the critical temperatures we use finite-size scaling (FSS) [52] analysis of the susceptibilities $\chi_X(\bar{T}; L)$ of the order parameters $X = \theta$ and Q [Eq. (11)], the specific heat at constant volume $c_V(\bar{T}; L)$ [Eq. (12)], and isothermal compressibility [Eq. (13)].

Figure 11 shows simulation results for the order parameters, Q and θ ; susceptibilities, χ_Q and χ_θ , specific heat c_V , and isothermal compressibility κ for chemical potential $\bar{\mu} = 2.3$. For clarity, error bars are not shown in the figure. The susceptibility, specific heat and isothermal compressibility exhibit signatures of a continuous transition. In all cases the peaks increase systematically with system size. Similar results are obtained for $\bar{\mu} = 2.4, 2.5, 2.6, 5.0$, and 10 . As the chemical potential is increased, the maxima shift to higher temperatures, approaching the value $\bar{T}_{c, \bar{\mu} \rightarrow \infty}^* = 0.9526$ reported in Ref. [41]. This behavior confirms that the DF-HDL line is continuous, in agreement with the TM calculations from Sec. III C.

Using the results for χ_Q, χ_θ, c_V , and κ we estimate the critical temperature \bar{T}_c^* . Initially, we estimate the size dependent pseudocritical temperature \bar{T}_c through a polynomial fit to the data near the maximum, as described in the preceding subsection.

The pseudocritical temperatures \bar{T}_c for $\bar{\mu} = 2.3$ are plotted versus $1/L$ in Fig. 12. Similar results were obtained for $\bar{\mu} = 2.4, 2.5, 2.6, 5.0$, and 10 . The set of pseudocritical temperatures appear to converge as $L \rightarrow \infty$ for all the studied values of $\bar{\mu}$. The global estimate of \bar{T}_c^* was obtained through a weighted average with weight $1/\sigma^2$, where σ represents the uncertainty of each quantity. The final estimates of \bar{T}_c^* are the squares in the phase diagram Fig. 15.

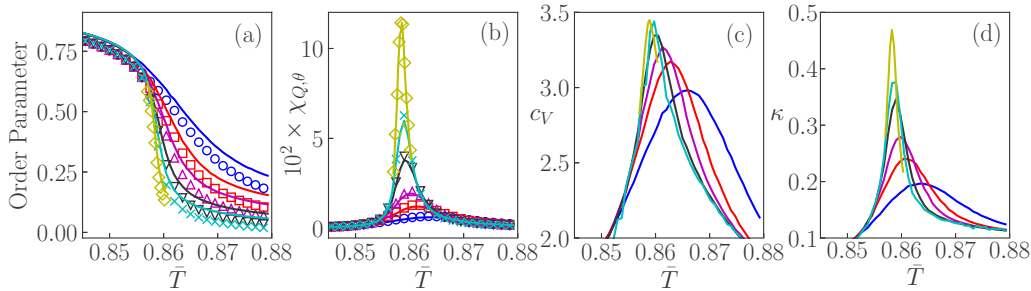


FIG. 11. (a) Order parameters Q and θ , (b) susceptibilities χ_Q and χ_θ , (c) specific heat c_V , and (d) isothermal compressibility versus \bar{T} for $\bar{\mu} = 2.3$. The system sizes [for curves from lower to upper in panels (b-d) and upper to lower in panel (a)] are $L = 32, 48, 64, 96, 128$, and 192 . The order parameter Q and its susceptibility χ_Q are represented by solid lines, θ and χ_θ by symbols.

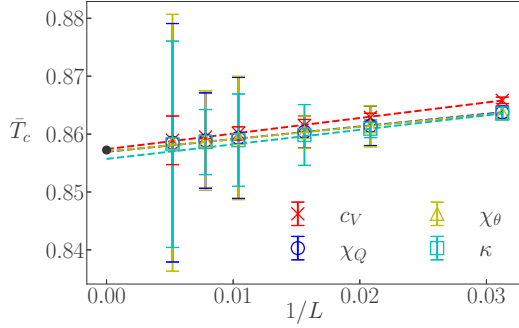


FIG. 12. Pseudocritical temperatures associated with, c_v , χ_Q , χ_θ , and κ , with symbols as indicated, versus $1/L$ for $\bar{\mu} = 2.3$. Dash lines are linear fits to the data and the filled black dot indicates the global estimate for the critical temperature \bar{T}_c^* .

D. Critical exponents

For $\bar{\mu} = 2.3$ and 10, we estimate the critical-exponent ratios β/ν and γ/ν from fits to the data for $Q(\bar{T}_c^*)$, $\theta(\bar{T}_c^*)$, $\chi_Q(\bar{T}_c^*)$, and $\chi_\theta(\bar{T}_c^*)$ versus system size (see Fig. 13). From the linear fits, and including the effect of the uncertainty in \bar{T}_c^* , we obtained the estimates in Table V. The values for these ratios for the two-dimensional, three-state Potts model are $\beta_{\text{Potts}}/\nu_{\text{Potts}} = 2/15 = 0.1333\dots$ and $\gamma_{\text{Potts}}/\nu_{\text{Potts}} = 26/15 = 1.7333\dots$. In the worst cases, the discrepancy is about 6% for $\mu = 2.3$ and 8% for $\mu = 10$.

Figure 14 shows the linear fit for $\ln c_v(\bar{T}_c)$ for $\mu = 10.0$, yielding the estimate $\alpha/\nu = 0.44(1)$, i.e., a discrepancy with the ratio for the two-dimensional, three-state Potts model $\alpha/\nu_{\text{Potts}} = 0.4$ of 10%. For $\bar{\mu} = 2.3$, the discrepancy in this ratio is 73%. We believe this huge difference is likely due to finite-size corrections that are more important close to the CEP ($\bar{\mu}_{\text{cep}} = 1.9498$) where the DF-HDL line encounters the LDL-HDL and DF-LDL lines.

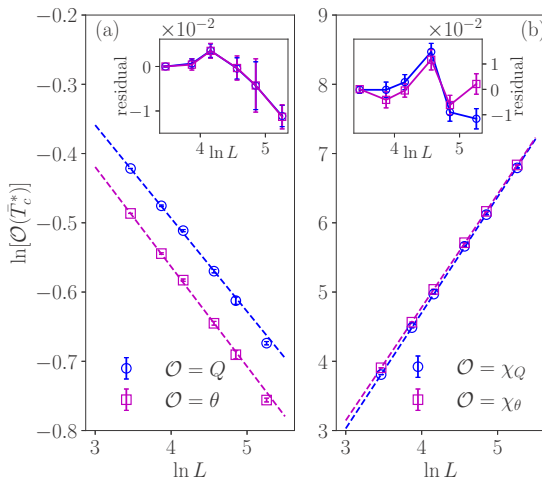


FIG. 13. (a) Order parameter Q (θ) versus system size for $\bar{\mu} = 2.3$. The circles (squares) are the simulation data; dashed lines are least-squares linear fits of the data. Inset shows the residuals of the fits. (b) Analogous plots for the susceptibilities χ_Q (χ_θ).

TABLE V. Estimates of the ratios β/ν , γ/ν and α/ν for chemical potentials $\bar{\mu} = 2.3$ and 10.

| $\bar{\mu}$ | β_Q/ν | β_θ/ν | γ_Q/ν | γ_θ/ν | α/ν |
|-------------|---------------|--------------------|----------------|---------------------|--------------|
| 2.3 | 0.126(7) | 0.136(8) | 1.66(4) | 1.63(4) | 0.11(1) |
| 10.0 | 0.126(7) | 0.122(7) | 1.75(5) | 1.75(4) | 0.44(1) |

V. DISCUSSION

Figure 15(a) shows the phase diagram of the symmetric ALG model in the $\bar{\mu}$ - \bar{T} plane, summarizing the results reported above. The predictions of the TM analysis are in very good quantitative agreement with MC simulation. In fact, the maximum difference between the estimates from each method is smaller than 2% along the LDL-HDL coexistence line and, notably, is at most 0.1% for the DF-HDL and DF-LDL lines. The natures of the transitions are also the same in both cases. This remarkable agreement confirms that we are accessing the correct thermodynamic behavior of the model.

Our results demonstrate that the DF-LDL transition is always discontinuous, without any critical or multicritical point. This is confirmed by the absence of a crossing in the pseudocritical transition lines from the TM analysis, by the bimodal histograms in MC simulations and also in the phase diagram of temperature versus total density ($\bar{T} - \rho$), depicted in Fig. 15(b). This diagram makes it clear that the densities are discontinuous at the DF-LDL transition line up to temperatures very close to the turning point (in the $\bar{\mu} - \bar{T}$ diagram), which is located at $\bar{T}_t \approx 0.983$ and $\bar{\mu}_t \approx 0.31$. It is, however, difficult to estimate the densities accurately very near this point, since ρ_{DF} becomes very similar to ρ_{LDL} . This strongly suggests that $\rho_{\text{DF}} = \rho_{\text{LDL}}$ at the point $(\bar{T}_t, \bar{\mu}_t)$ — as observed in the Husimi lattice solution of this model [34], which furnishes a $(\bar{T} - \rho)$ diagram very similar to the one found here (see Fig. 4(a) of Ref. [34])—even though this is certainly not a critical point. In fact, the pressure versus temperature ($\bar{P} - \bar{T}$) diagram of the model is qualitatively very similar to the $(\bar{\mu} - \bar{T})$ one in Fig. 15, also displaying a turning point in the DF-LDL transition line at some pressure \bar{P}_t [22,34,35]. Then, from the Clausius-Clapeyron equation one has $\rho_{\text{DF}} < \rho_{\text{LDL}}$ for $\bar{\mu} < \bar{\mu}_t$, and $\rho_{\text{DF}} > \rho_{\text{LDL}}$ for $\bar{\mu} > \bar{\mu}_t$,

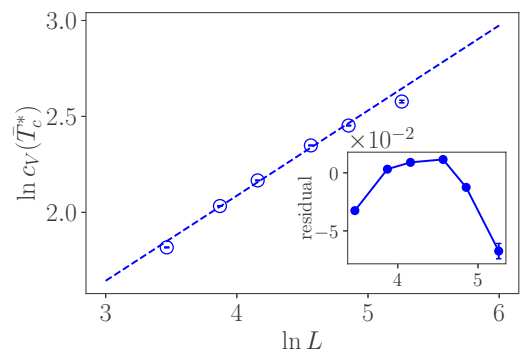


FIG. 14. Specific heat c_v versus system size at critical temperature for $\bar{\mu} = 10.0$. The circles are the simulation data; the dashed line is a least-squares linear fit of the data. Inset shows the residuals of the fit.

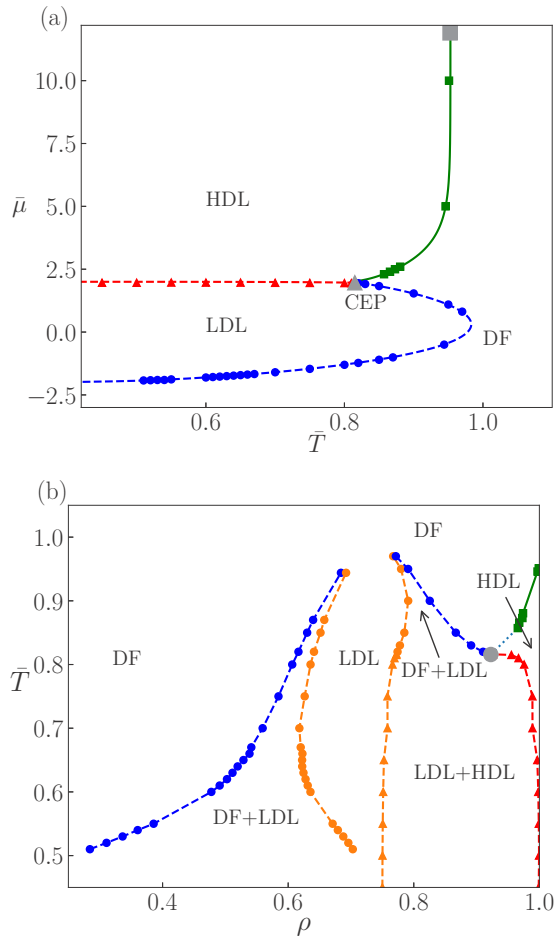


FIG. 15. Phase diagram for the symmetric ALG model in the $\bar{\mu} \times \bar{T}$ plane (a) and the $\bar{T} \times \rho$ plane (b). Symbols are results from Monte Carlo (MC) simulations. Dashed lines represent discontinuous transitions and solid ones continuous transitions. Only in (a) lines are results obtained using Transfer Matrix (TM) calculations. The gray triangle marks the location of the critical end point (CEP) estimated using TM and the gray square marks the location of the critical point in the limit $\bar{\mu} \rightarrow \infty$ obtained via MC simulations in Ref. [41]. The gray circle in (b) marks the density at $\bar{\mu} = 1.95$ (for $L = 128$), very close to our estimate of $\bar{\mu}_{\text{cep,MC}} = 1.9498(6)$. The green dotted line is a conjecture as to how the critical line meets the CEP.

as indeed observed in Fig. 15(b), provided that the entropies follow $s_{\text{DF}} > s_{\text{LDL}}$, along the coexistence line, as it is quite expected. This very same condition yields $\rho_{\text{DF}} = \rho_{\text{LDL}}$ at $(\bar{T}_t, \bar{\mu}_t)$, but, in turn, it indicates that this is not a critical point, since $s_{\text{DF}} \neq s_{\text{LDL}}$ there. Importantly, these results provide compelling evidence that the entire DF-LDL transition

line is discontinuous, ruling out a critical point at $\bar{T} \approx 0.55$ or a tricritical point at $\bar{T} \approx 0.65$, as claimed in previous MC analyses in Refs. [22,35], respectively.

Also in contrast with earlier simulations, we find a critical line separating the DF and HDL phases. This line meets the LDL-HDL and DF-LDL coexistence lines at a critical end point (CEP). This shows that the point where the LDL-HDL coexistence line ends—reported in literature as critical [22], triple [34], and tricritical [35]—is actually a CEP. Therefore, although this ALG model has an interesting phase behavior, beyond displaying some thermodynamic anomalies, it is not a good model for liquid water, as initially suggested, because it has neither a liquid-gas coexistence line ending at a critical point, nor a LLCP. In light of the discussion in the Introduction, it seems that absence of a LLCP is a general feature of lattice models with attractive orientational interactions competing with “van der Waals” repulsion between first neighbor molecules.

Although determining the universality class of the continuous transitions displayed by models for water is key to establish a full connection with the actual behavior of water, this has not been widely investigated, perhaps because the very nature of these transitions are the subject of controversy. A recent account of these critical properties for realistic models can be found in Ref. [53]. For lattice models, some examples include the debate in the literature on the critical exponents of the liquid-liquid transition in the classic Bell-Lavis model [54,55], and our previous study of the present ALG model in the fully occupied limit, where the DF-HDL transition was found to be in the 3-state Potts class. The central charge obtained here, deviating by $\sim 1\%$ from the Potts value, gives additional evidence of this. The scaled gaps, however, present a large deviation from those of the 3-state Potts class. The analysis of the central charge for finite chemical potentials indicates that it converges to the same value along the entire DF-HDL critical line. Nevertheless, finite-size corrections become very strong as $\bar{\mu}$ approaches $\bar{\mu}_{\text{cep}} = 1.9597(8)$. This certainly explains why some critical exponent ratios estimated in simulations for $\bar{\mu} = 2.3$ exhibit considerable deviations from the Potts values, while for $\bar{\mu} = 10$ the deviations are much smaller. Despite this, the overall picture suggests that this order-disorder transition is always in the 3-state Potts class, as is expected from its threefold (S_3) symmetry breaking.

ACKNOWLEDGMENTS

Authors acknowledge financial support from CNPq (R.D. under Grant No. 303766/2016-6; and T.J.O.), CAPES (I.I. and A.P.F.), and Fundação de Amparo à Pesquisa do Estado de Minas Gerais (T.J.O.).

- [1] H. E. Stanley (ed.), *Liquid Polymorphism: Advances in Chemical Physics* (Wiley, NY, 2013), Vol. 152.
- [2] R. J. Speedy and C. A. Angell, Isothermal compressibility of supercooled water and evidence of a singularity at -45°C , *J. Chem. Phys.* **65**, 851 (1976).
- [3] S. Sastry, P. G. Debenedetti, F. Sciortino, and H. E. Stanley, Singularity-free interpretation of the thermody-

namics of supercooled water, *Phys. Rev. E* **53**, 6144 (1996).

- [4] P. H. Poole, F. Sciortino, U. Essmann, and H. E. Stanley, Phase behavior of metastable water, *Nature (London)* **360**, 324 (1992).
- [5] O. Mishima, L. D. Calvert, and E. Whalley, An apparently 1st-order transition between 2 amorphous phases of ice induced by pressure, *Nature (London)* **314**, 76 (1985).

- [6] R. M. Lynden-Bell, S. C. Morris, J. D. Barrow, J. L. Finney, and C. L. Harper, Jr. (eds.), *Water and Life: The Unique Properties of H₂O* (CRC Press, Boca Raton, FL, 2010).
- [7] A. K. Soper and M. A. Ricci, Structures of High-Density and Low-Density Water, *Phys. Rev. Lett.* **84**, 2881 (2000).
- [8] O. Mishima and H. E. Stanley, Decompression-induced melting of ice IV and the liquid-liquid transition in water, *Nature (London)* **392**, 164 (1998).
- [9] S. Woutersen, B. Ensing, M. Hilbers, Z. Zhao, and C. A. Angell, A liquid-liquid transition in supercooled aqueous solution related to the HDA-LDA transition, *Science* **359**, 1127 (2018).
- [10] L. Liu, S.-H. Chen, A. Faraone, C.-W. Yen, and C.-Y. Mou, Pressure Dependence of Fragile-To-Strong Transition and a Possible Second Critical Point in Supercooled Confined Water, *Phys. Rev. Lett.* **95**, 117802 (2005).
- [11] S.-H. Chen, F. Mallamace, C.-Y. Mou, M. Broccio, C. Corsaro, A. Faraone, and L. Liu, Violation of the Stokes-Einstein relation in supercooled water, *Proc. Natl. Acad. Sci. USA* **103**, 12974 (2006).
- [12] F. Mallamace, M. Broccio, C. Corsaro, A. Faraone, D. Majolino, V. Venuti, L. Liu, C.-Y. Mou, and S.-H. Chen, Evidence of the existence of the low-density liquid phase in supercooled, confined water, *Proc. Natl. Acad. Sci. USA* **104**, 424 (2007).
- [13] F. Mallamace, The liquid water polymorphism, *Proc. Natl. Acad. Sci. USA* **106**, 15097 (2009).
- [14] A. K. Soper, Is water one liquid or two? *J. Chem. Phys.* **150**, 234503 (2019).
- [15] J. C. Palmer, P. H. Poole, F. Sciortino, and P. G. Debenedetti, Advances in computational studies of the liquid-liquid transition in water and water-like models, *Chem. Rev.* **118**, 9129 (2018).
- [16] G. M. Bell and D. A. Lavis, Two-dimensional bonded lattice fluids. I. Interstitial model, *J. Phys. A* **3**, 427 (1970).
- [17] G. M. Bell and D. A. Lavis, Two-dimensional bonded lattice fluids. II. Orientable molecule model, *J. Phys. A* **3**, 568 (1970).
- [18] D. A. Huckaby and R. S. Hanna, A two-dimensional lattice gas model for water, *J. Phys. A* **20**, 5311 (1987).
- [19] A. Patrykiewicz, O. Pizio, and S. Sokółowski, Novel Phase Behavior in a Two-Dimensional Network-Forming Lattice Fluid, *Phys. Rev. Lett.* **83**, 3442 (1999).
- [20] C. Buzano, E. De Stefanis, A. Pelizzola, and M. Pretti, Two-dimensional lattice-fluid model with waterlike anomalies, *Phys. Rev. E* **69**, 061502 (2004).
- [21] V. B. Henriques and M. C. Barbosa, Liquid polymorphism and density anomaly in a lattice gas model, *Phys. Rev. E* **71**, 031504 (2005).
- [22] A. L. Balladares, V. B. Henriques, and M. C. Barbosa, Liquid polymorphism, density anomaly and H-bond disruption in associating lattice gases, *J. Phys.: Condens. Matter* **19**, 116105 (2007).
- [23] G. M. Bell, Statistical mechanics of water: Lattice model with directed bonding, *J. Phys. C* **5**, 889 (1972).
- [24] P. H. E. Meijer, R. Kikuchi, and E. V. Royen, Phase diagram of water based on a lattice model, *Physica A* **115**, 124 (1982).
- [25] D. A. Lavis and B. W. Southern, Renormalization group study of a three-dimensional lattice model with directional bonding, *J. Stat. Phys.* **35**, 489 (1984).
- [26] N. A. M. Besseling and J. Lyklema, Equilibrium properties of water and its liquid-vapor interface, *J. Phys. Chem.* **98**, 11610 (1994).
- [27] C. J. Roberts and P. G. Debenedetti, Polyamorphism and density anomalies in network-forming fluids: Zeroth- and first-order approximations, *J. Chem. Phys.* **105**, 658 (1996).
- [28] C. J. Roberts, A. Z. Panagiotopoulos, and P. G. Debenedetti, Liquid-Liquid Immiscibility in Pure Fluids: Polyamorphism in Simulations of a Network-Forming Fluid, *Phys. Rev. Lett.* **77**, 4386 (1996).
- [29] M. Pretti and C. Buzano, Thermodynamic anomalies in a lattice model of water, *J. Chem. Phys.* **121**, 11856 (2004).
- [30] M. Pretti and C. Buzano, Thermodynamic anomalies in a lattice model of water: Solvation properties, *J. Chem. Phys.* **123**, 024506 (2005).
- [31] S. Sastry, F. Sciortino, and H. E. Stanley, Limits of stability of the liquid phase in a lattice model with water-like properties, *J. Chem. Phys.* **98**, 9863 (1993).
- [32] S. S. Borick, P. G. Debenedetti, and S. Sastry, A lattice model of network-forming fluids with orientation-dependent bonding: Equilibrium, stability, and implications for the phase behavior of supercooled water, *J. Phys. Chem.* **99**, 3781 (1995).
- [33] M. Girardi, A. L. Balladares, V. B. Henriques, and M. C. Barbosa, Liquid polymorphism and density anomaly in a three-dimensional associating lattice gas, *J. Chem. Phys.* **126**, 064503 (2007).
- [34] T. J. Oliveira, J. F. Stilck, and Marco Aurelio A. Barbosa, Solution of an associating lattice-gas model with density anomaly on a husimi lattice, *Phys. Rev. E* **82**, 051131 (2010).
- [35] A. P. Furlan, C. E. Fiore, and M. C. Barbosa, Influence of disordered porous media on the anomalous properties of a simple water model, *Phys. Rev. E* **92**, 032404 (2015).
- [36] C. Buzzano, E. De Stefanis, and M. Pretti, Cluster-variation approximation for a network-forming lattice-fluid model, *J. Chem. Phys.* **129**, 024506 (2008).
- [37] M. Pretti, C. Buzzano, and E. De Stefanis, Revisiting waterlike network-forming lattice models, *J. Chem. Phys.* **131**, 224508 (2009).
- [38] M. M. Szortyka, M. Girardi, V. B. Henriques, and M. C. Barbosa, Dynamic transitions in a three-dimensional associating lattice gas model, *J. Chem. Phys.* **132**, 134904 (2010).
- [39] M. M. Szortyka, V. B. Henriques, M. Girardi, and M. C. Barbosa, Dynamic transitions in a two-dimensional associating lattice gas model, *J. Chem. Phys.* **130**, 184902 (2009).
- [40] A. P. Furlan, N. G. Almarza, and M. C. Barbosa, Lattice model for water-solute mixtures, *J. Chem. Phys.* **145**, 144501 (2016).
- [41] A. P. Furlan, T. J. Oliveira, J. F. Stilck, and R. Dickman, Order-disorder transition in a two-dimensional associating lattice gas, *Phys. Rev. E* **100**, 022109 (2019).
- [42] F. Y. Wu, The Potts model, *Rev. Mod. Phys.* **54**, 235 (1982).
- [43] W. Guo and H. W. J. Blöte, Finite-size analysis of the hard-square lattice gas, *Phys. Rev. E* **66**, 046140 (2002).
- [44] T. J. Oliveira and J. F. Stilck, Transfer-matrix study of a hard-square lattice gas with two kinds of particles and density anomaly, *Phys. Rev. E* **92**, 032101 (2015).
- [45] M. E. Fisher, in *Proceedings of International School of Physics "Enrico Fermi,"* edited by M. S. Green (Academic Press, New York, 1971).
- [46] H. W. J. Blöte, J. L. Cardy, and M. P. Nightingale, *Phys. Rev. Lett.* **56**, 742 (1986); I. Affleck, *ibid.* **56**, 746 (1986).

- [47] S. L. A. de Queiroz, Finite-size scaling corrections in two-dimensional Ising and Potts ferromagnets, *J. Phys. A: Math. Gen.* **33**, 721 (2000).
- [48] P. A. Rikvold, W. Kinzel, J. D. Gunton, and K. Kaski, Finite-size-scaling study of a two-dimensional lattice-gas model with a tricritical point, *Phys. Rev. B* **28**, 2686 (1983).
- [49] N. C. Bartelt, T. L. Einstein, and L. D. Roelofs, Transfer-matrix approach to estimating coverage discontinuities and multicritical-point positions in two-dimensional lattice-gas phase diagrams, *Phys. Rev. B* **34**, 1616 (1986).
- [50] J. C. Xavier, F. C. Alcaraz, D. Pena Lara, and J. A. Plascak, Critical behavior of the spin-3/2 Blume-Capel model in two dimensions, *Phys. Rev. B* **57**, 11575 (1998).
- [51] M. Jung and D.-H. Kim, First-order transitions and thermodynamic properties in the 2D Blume-Capel model: The transfer-matrix method revisited, *Eur. Phys. J. B* **90**, 245 (2017).
- [52] M. P. Allen and D. J. Tildesley, *Computer Simulation of Liquids*, Oxford Science Publications (Clarendon Press, Oxford, UK, 1989).
- [53] P. G. Debenedetti, F. Sciortino, and G. H. Zerze, Second critical point in two realistic models of water, *Science* **369**, 289 (2020).
- [54] C. E. Fiore, M. M. Szortyka, M. C. Barbosa, and V. B. Henriques, Liquid polymorphism, order-disorder transitions and anomalous behavior: A Monte Carlo study of the Bell-Lavis model for water, *J. Chem. Phys.* **131**, 164506 (2009).
- [55] M. Simenas, A. Ibenskas, and E. E. Tornau, Phase transition properties of the Bell-Lavis model, *Phys. Rev. E* **90**, 042124 (2014).